

Research article

Hyeon Bo Shim and Jae W. Hahn*

Plasmonic near-field scanning nanoscope with a cross-polarization detection technique

<https://doi.org/10.1515/nanoph-2019-0132>

Received May 2, 2019; revised June 21, 2019; accepted July 1, 2019

Abstract: A cross-polarization detection technique was introduced to enhance the signal-to-noise ratio (SNR) of a plasmonic near-field scanning nanoscope (PNSN) using the anisotropic reflection from a metallic ridge nano-aperture. Assuming that the nano-aperture is an resistor-inductor-capacitor-equivalent circuit, we propose an analytic circuit model to quantitatively predict the relationship between the copolarization and cross-polarization signals of the PNSN. It was found that the magnitude of the cross-polarization signal has an opposite trend with respect to the copolarization signal, providing a larger PNSN signal. We demonstrated the PNSN with dual channels for detecting both polarization signals. The performance of the PNSN was characterized by recording images of heterogeneous nanostructures in dynamic random access memory patterns and we enhanced the SNR of the images by a factor of 2.7–4.9.

Keywords: plasmonic nanoscope; plasmonic resonance; ridge nano-antenna; ridge nano-aperture; cross-polarization detection; equivalent circuit.

1 Introduction

A metallic ridge nano-aperture is a common optical component that provides a large transmission and highly focused spot in the sub-wavelength scale region due to its plasmonic resonance behavior [1–4]. Because of their potential to create highly restricted optical hot spots and provide extraordinary transmittance, despite the very

small aperture size, ridge nano-apertures are used extensively in many applications in various research fields, such as nanoscale near-field patterning, near-field scanning optical microscopy, plasmonic enhanced sensing, and optical tweezers [5–9]. The ridge nano-aperture is also applicable to sensing or detecting techniques such as plasmonic sensors and plasmonic near-field scanning nanoscope (PNSN) using the resonance characteristics of the aperture, which is highly sensitive to the surroundings [10–12]. By measuring the reflected beam from the nano-aperture, the PNSN can record images of heterogeneous nanostructures and detect buried objects.

Since optical instruments that use a scanning optical probe are strongly affected by the motional noise generated during scanning, the elimination of the motional noise in the optical signal is necessary to enhance the contrast of the image. Noise reduction using the cross-polarization detection technique has been studied to enhance the signal-to-noise ratio (SNR) of optical signals, or contrast-to-noise ratio of optical images [13–22]. However, the generation of the cross-polarization signal is reported for limited situations; multiple scattering media such as biological tissue [13–16], very small scatter such as a scanning probe or nanoparticle [17–20], or optical-electrical interacting structures such as nanoantenna [19, 21, 22]. Also, due to the small interactive areas, the cross-polarization signal generated by plasmonic antenna or nanoparticles is very small compared with the incident or background. Moreover, since most of these techniques detect the optical far-field from the target structure [13–16, 18, 20–22], the cross-polarization detection technique does not ensure nanoscale spatial resolution. The cross-polarization detection technique [19] has rarely been applied to optical instruments that detect nanoscale structures with a metallic ridge nano-aperture.

Since a metallic nano-aperture has a nonlinear response and polarization sensitivity to the incident beam [23–27], we can expect the reflected beam from the nano-aperture to have a cross-polarization component due to the anisotropic reflection from the nano-aperture. PNSN records the change in the reflection intensity from the scanning nano-aperture as a signal,

*Corresponding author: Jae W. Hahn, Nano Photonics Laboratory, School of Mechanical Engineering, Yonsei University, 50 Yonsei-ro, Seodaemun-gu, Seoul 03722, Republic of Korea, e-mail: jaewhahn@yonsei.ac.kr. <https://orcid.org/0000-0003-2745-9973>

Hyeon Bo Shim: Nano Photonics Laboratory, School of Mechanical Engineering, Yonsei University, 50 Yonsei-ro, Seodaemun-gu, Seoul 03722, Republic of Korea

and the cross-polarization component of the reflected light from the aperture is inversely related to the total reflected light, giving a negative signal. Unfortunately, theoretical approaches to understanding the generation of cross-polarization reflection from the complicated nanostructures are limited. Most research on the ridge nano-aperture has been focused on transmission due to its relevance in resonance transmission and the generation of highly focused optical near-field spots. Transmission and reflection at the nano-aperture exhibit opposite responses, and the main component of the transmitted beam is copolarized with the incident beam. Therefore, in order to realize the cross-polarization detection technique for PNSN, in-depth studies on reflected light from the ridge nano-aperture, especially theoretical analysis of both the copolarization and cross-polarization components in the reflected beam, need to be carried out.

In this study, we introduced a theoretical model based on the resistor-inductor-capacitor-equivalent circuit to analyze plasmonic resonance and predict reflection signals from the ridge nano-aperture by assuming the plasmon interaction as an oscillating current. We calculated the electric properties and resonance characteristics of the nano-aperture with simplified geometry to apply our theory directly to different dimensions, and quantitatively obtained the characteristics of the reflection from the ridge nano-aperture in terms of the behavior of two polarization components of the reflected beam. Combining two channel detection systems for the dual polarization of the reflected beam, we implemented the cross-polarization detection technique for the PNSN system. Also, the enhancement of the SNR of the image data was evaluated by recording pattern images of heterogeneous nanostructures with the PNSN system.

2 Theory and methods

We assumed that the origin of the anisotropic reflection from the ridge nano-aperture has a different mechanism for each polarization. Figure 1 shows the schematic of the mechanism of generation of each component in the reflected beam that explains the source of the anisotropic reflection. Copolarization reflection is the intrinsic system reflection that has a trade-off relation with resonant transmission, which produces weak reflection under the resonance conditions of the ridge nano-aperture. In contrast, cross-polarization reflection becomes stronger under the resonance conditions because it is generated by the perpendicular portion of the oscillating resonant current,

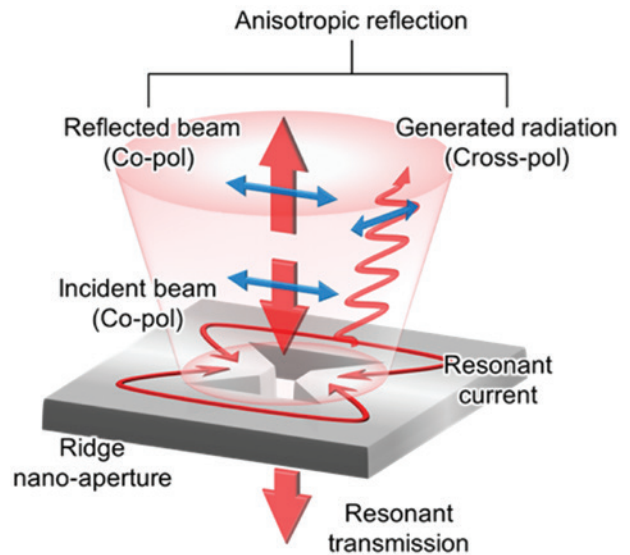


Figure 1: Schematic of the anisotropic reflection from a ridge nano-aperture.

The direction of each polarization is represented by blue arrows. When the aperture is illuminated by a linearly polarized beam which is parallel to the aperture ridge (copolarization), a plasmonic resonance occurs by the interaction between the aperture and the incident light. This resonance creates a resonant transmission that passes through the aperture and a resonant current that oscillates around the aperture outline. Copolarization reflection shows a negative correlation with the resonance, because the reflection and resonant transmission have a trade-off relationship with each other. On the contrary, cross-polarization reflection shows a positive correlation with the resonance, because it is generated by radiation from the perpendicular component of an oscillating resonance current induced by the plasmonic resonance.

which is orthogonal to the incident polarization around the aperture outline. As the opposite trend of the anisotropic reflection becomes key to enhancing the SNR of the detection system, which uses the ridge nano-aperture, we deeply analyzed this trend of reflection signal variations of each polarization depending on the identical resonance conditions.

In order to analyze the mechanisms of the anisotropic reflection of the ridge nano-aperture in detail, we introduced an equivalent electric circuit model, because the oscillation of electrons in a metallic ridge nano-aperture interacting with the incident light is equal to the oscillation of the electric current. Therefore, we can replace the aperture system with an equivalent electrical circuit which includes resistance, inductance, and capacitance to analyze the resonance characteristics of the aperture. Subsequently, we can derive the reflectance or transmittance of the aperture system using the equivalent electrical circuit by applying the transmission line theory [28, 29]. Expanding this

equivalent electrical circuit model, we suggest a methodology for the quantitative analysis of the anisotropic reflection including both copolarization and cross-polarization reflection signals from the ridge nano-aperture.

The entire equivalent electric circuit composed of the ridge nano-aperture system, input space, and output space is shown in Figure 2. The circuit of the aperture highlighted by the red box is composed of the parallel connection of the resistor-inductor series and a capacitor, which have values of $R_{\text{tot}} = 6.22 \Omega$, $L_{\text{tot}} = 36.2 \text{ fH}$, and $C_{\text{tot}} = 3.37 \text{ aF}$, respectively. Each value of the electronic component is calculated quantitatively by assuming the aperture to be a simplified wire loop, as described in the Supplementary Material. The resistance is calculated simply from the resistivity, the inductance is calculated using the Biot-Savart law, and the capacitance is calculated based on the split-ring resonator model. Consequently, the system impedance of the aperture becomes $Z = (R_{\text{tot}} + j\omega L_{\text{tot}}) || (j\omega C_{\text{tot}})^{-1}$. Here, ω is the angular frequency of the oscillating current identical to the angular frequency of the incident light. The values of the electronic components were calculated quantitatively by using the geometry of the simplified wire loop for the ridge nano-aperture, as described in the supporting information. In addition, the characteristic impedance of the output space is defined as $Z_1 = Z_0/n$, where the refractive index of the output space is n and the characteristic impedance of the free space is Z_0 . Here, V_0 is the input voltage and i_1 is the induced current on the aperture system with respect to the transmitted load voltage V_1 , which is applied on the node of the aperture system. We calculated the reflection and transmission coefficients of the aperture system, i.e. Γ and τ , respectively, by using the transmission line theory for combined impedance, $Z' = Z || Z_1$, as shown in Eqs. (1) and (2):

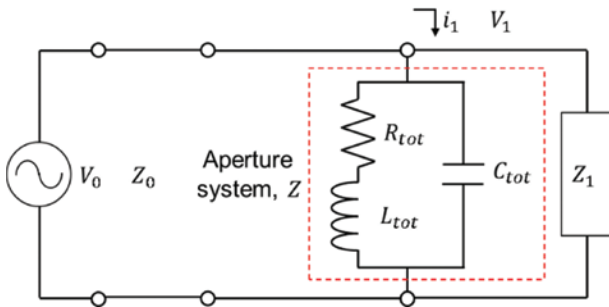


Figure 2: The equivalent electric circuit of an entire ridge nano-aperture system including input and output space. The aperture system highlighted by a red box consists of the resistor-inductor series and the capacitor connected in parallel. The incident wave that comes from the input space (free space) passes through the aperture system into the output space.

$$\Gamma = \frac{Z' - Z_0}{Z' + Z_0} \quad (1)$$

$$\tau = 1 + \Gamma = \frac{2Z'}{Z' + Z_0} \quad (2)$$

As Z is very large under the resonance conditions and Z_1 is smaller than Z_0 because $n > 1$, the combined impedance is smaller than the free-space impedance. Note that the absolute values of these two coefficients, $|\Gamma|$ and $|\tau| = 1 - |\Gamma|$ show a trade-off relationship with respect to a change in n , because the reflection coefficient shows a boundary of $-1 < \Gamma < 0$, which is derived from $Z' < Z_0$.

Based on these reflection and transmission coefficients, we calculated the anisotropic reflection for each polarization component. We need to calculate the induced current i_1 , which flows around the nano-aperture, because a cross-polarization reflection is generated from the oscillating current induced by the incident beam, as mentioned earlier. It is simply driven by the ratio of the transmitted load voltage and impedance of the aperture, as shown in Eq. (3). Note that the induced current is proportional to the transmission coefficient τ :

$$i_1 = \frac{V_1}{Z} = \frac{\tau V_0}{Z} \quad (3)$$

To determine the anisotropic reflection intensity, we split this intensity into a variance term and offset. Because the interaction with the aperture does not occur for the entire incident light, we employed a weight factor η , which indicates a ratio between the interacted light with the aperture to the incident light. The factor is calculated from the geometrical integration of the horizontal component of polarization of the focused incident beam, as described in the supporting information. Further, because another portion of the light does not interact and is simply reflected off the metal surface, we set the offset as products of $(1 - \eta)$ and intrinsic reflectances of a flat metal surface without an aperture for the copolarization and cross-polarization, R_{co0} and $R_{\text{co'0}}$, respectively. As the reflectance is defined as the ratio of reflected power $V_0^2/2Z_0$ to incident power $(\Gamma V_0)^2/2Z_0$, we can define the copolarization reflection intensity I_{co} , which shows a linear trend with reflectance Γ^2 as:

$$I_{\text{co}} = \eta \Gamma^2 + (1 - \eta) R_{\text{co0}} \quad (4)$$

By contrast, because the field amplitude of the radiation from the aperture is proportional to the current on

the aperture system, we can define the cross-polarization reflection intensity I_{cr} , which varies linearly with transmittance τ^2 , as:

$$I_{cr} = \eta K \tau^2 + (1 - \eta) R_{cr0} \quad (5)$$

Here, K is the proportionality constant of the cross-polarization reflection intensity. We assume that η and K are fixed values from the geometry of the aperture.

From the calculated intensities of the anisotropic reflection, we subsequently define the copolarization and cross-polarization reflection signals, S_{co} and S_{cr} , respectively, as normalized values of the reflection intensity changes for both polarizations, as shown in Eqs. (6) and (7). Here, $I_{co}(0)$ and $I_{cr}(0)$ are the reflection intensities where the output space is the free space, for each polarization, respectively. Because the absolute values of reflection and transmission coefficient show an opposite trend with the change in the refractive index of the output space, we can easily grasp the opposite trend between the reflection signals for each polarization. Eventually, we can apply the anisotropic reflection as a detection signal of the PNSN system to enhance the SNR with a signal processing:

$$S_{co} = \frac{I_{co} - I_{co}(0)}{I_{co}(0)} = \frac{\eta}{I_{co}(0)} \Delta(|\Gamma|^2) \quad (6)$$

$$S_{cr} = \frac{I_{cr} - I_{cr}(0)}{I_{cr}(0)} = \frac{\eta K \Delta(\tau)^2}{I_{cr}(0)} = \frac{\eta K}{I_{cr}(0)} \Delta(1 - |\Gamma|^2) \quad (7)$$

By applying a cross-polarization-detection technique, we established a dual-channel detection system of PNSN to enhance the SNR performance of the system; this can individually collect two polarizations of the anisotropic reflection from the ridge nano-aperture. As shown in Figure 3, a portion of the incident beam separated by the first polarized beam splitter (PBS) becomes the reference beam. This reference beam is divided again by the beam splitter into the copolarization and cross-polarization reference beams. The other portion of the input beam is illuminated into the ridge nano-aperture through the reflection from the second PBS passing through the optical isolator composed of a Faraday rotator and a half-wave plate, to isolate the reflection and incident beams. The anisotropic reflection beam from the aperture, which consists of the copolarization and cross-polarization reflection beams, is separated by a second PBS; the copolarization reflection beam is reflected into the isolator, while the cross-polarization reflection beam is transmitted. These two separated beams are coupled in the optical

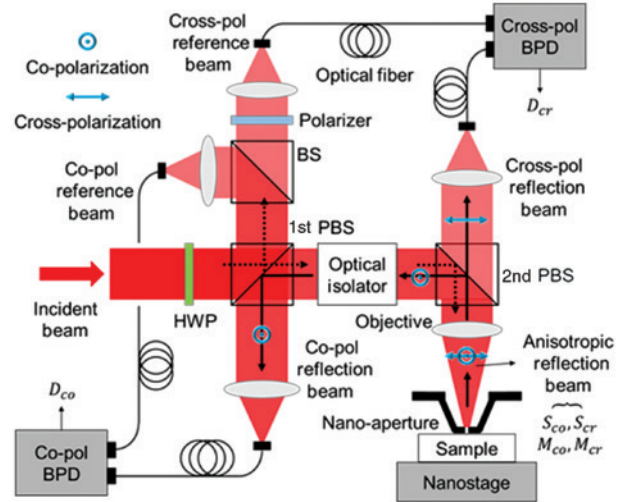


Figure 3: Schematic of a plasmonic near-field scanning nanoscope (PNSN) which collects both polarization components of the anisotropic reflection from the nano-aperture by applying a cross-polarization detection technique.

The incident beam, slightly rotated by a half-wave plate (HWP), is separated by the first polarized beam splitter (PBS) into the reference beam and the illumination beam. The reference beam is separated again by the beam splitter (BS) into copolarization and cross-polarization reference beams for each detection channel of the balanced photodetector (BPD). The second PBS separates the anisotropic reflection from the nano-aperture to detect each polarization component individually. The anisotropic reflection contains the signals and motional noises for each polarization. Black dashed arrows and solid arrows indicate the directions of the incident beam and the reflected beam, respectively, from the aperture.

fiber by using corresponding fiber couplers with the same structure. We can cancel out the offsets of both polarization reflection beams by using a balanced photodetector (BPD) for each detection channel. The gain of these reference beams for each polarization is tuned by rotating the half-wave plate and polarizer. For each polarization, the anisotropic reflection beam contains not only reflection signals S_{co} and S_{cr} , but also motional noises M_{co} and M_{cr} from the probe due to a contact scanning system. The ridge nano-aperture used in our experiment is made with an Al film by using the focused ion-beam-milling process with the following dimensions: the aperture outline (i.e. l_1 in Supplementary Material) is 135 nm, the metal thickness is 100 nm, and the aperture gap is 20 nm. It is found that the signal of the PNSN described in Eqs. (6–8) strongly depends on the resonance conditions of the ridge nano-aperture [11]. The aperture outline is determined by a theoretical calculation to set the resonance wavelength to 660 nm, as described in Supporting Information (see Figure S2).

The signal of the PNSN was processed after the detection of each polarization signal by each channel of the BPD. The copolarization BPD signal $D_{co} = C_{co} I_0 (S_{co} + M_{co})$ and the cross-polarization BPD signal $D_{cr} = C_{cr} I_0 (S_{cr} + M_{cr})$ are given as the difference between the reflected and reference beams. Each BPD signal contains the anisotropic reflection signal and motional noise. Here, C_{co} and C_{cr} are efficiencies of the optical components corresponding to each polarization reflection beam and I_0 is the power of the incident beam. Two different behaviors were observed between the reflection signals and motional noises for each polarization component of the anisotropic reflection. The reflection signals for each polarization showed opposite trends, because the change of copolarization reflection showed a positive relationship and cross-polarization reflection showed a negative relationship with the change of refractive index of the output space. On the contrary, the motional noises for each polarization showed the same trend because they occurred from the same probe, and each beam was collected by fiber couplers with the same structure. As a result, we obtained a PNSN signal processed with dual channel signals D_D , that is, the subtraction between two BPD signals for the different polarizations, as shown in Eq. (8):

$$D_D = D_{co} - GD_{cr} = C_{co} I_0 (S_{co} - R_M S_{cr}) \quad (8)$$

Here, a gain between the BPD signals is defined as $G = R_M \cdot C_{co} / C_{cr}$ for a ratio of the motional noise of each polarization channel; $R_M = M_{co} / M_{cr}$. The right side of Eq. 8 shows that the motional noise is canceled out in the dual-channel signal of the PNSN. In addition, the signal increases with the subtraction between each component because the change of each polarization component of the anisotropic reflection beam has an opposite trend. Consequently, the cancelation of the motional noises and the enlarged signal enhance the SNR of the PNSN signal from the ridge nano-aperture.

3 Results and discussion

We compared the anisotropic reflection signal for each polarization with respect to different refractive indices of the output space by using our circuit model and finite-difference time-domain (FDTD) simulation (Lumerical Inc., Vancouver, BC, Canada). The reflection signals show clear trends that have opposite directions to each other for both cases of the model (lines) and FDTD (symbols), as shown in Figure 4. Here, we calculated the weight factor

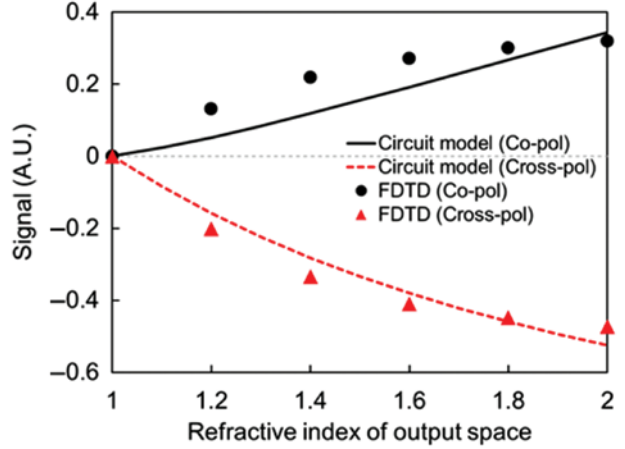


Figure 4: Variation of the anisotropic reflection signal for copolarization and cross-polarization components with respect to the refractive index of the output space. The black solid line and red dashed line indicate theoretical calculation results obtained using the circuit model for copolarization and cross-polarization, respectively. The black circle and red triangle indicate the finite-difference time-domain (FDTD) simulation for copolarization and cross-polarization, respectively.

$\eta = 0.68$, and set the proportional constant of cross-polarization reflection intensity $K = 0.01$ through curve fitting. Interestingly, the cross-polarization reflection signal (red dashed line and triangles) shows a larger contrast compared to the copolarization signal (black solid line and circles), with a change in the refractive index of the output space. This is because the copolarization reflection contains a larger background, as the background reflection is polarized in parallel to the incident beam. This opposite trend of the anisotropic reflection signal agrees with the prediction by the analytic form of the signals based on the characteristics of the reflection and transmission coefficients, as mentioned earlier [Eqs. (6) and (7)]. Furthermore, as the signals and refractive indices of the output space show a linear correlation for both polarizations in the opposite trend, we expect that the anisotropic reflection can enhance the SNR of a PNSN system successfully.

We performed experimentally the developed SNR performance of the PNSN which detects the anisotropic reflection signal from the ridge nano-aperture by imaging the heterogeneous structure in dynamic random access memory patterns with different refractive indices of 1 (air) and 1.46 (SiO_2). Figure 5A shows the two-dimensional signal map of the sample of a $3 \mu\text{m} \times 3 \mu\text{m}$ area for a dual-channel signal (left) and an individual polarization signal (right). The performance of SNR enhancement of the dual-channel signal compared with any other single polarization signal is obvious. The image of the

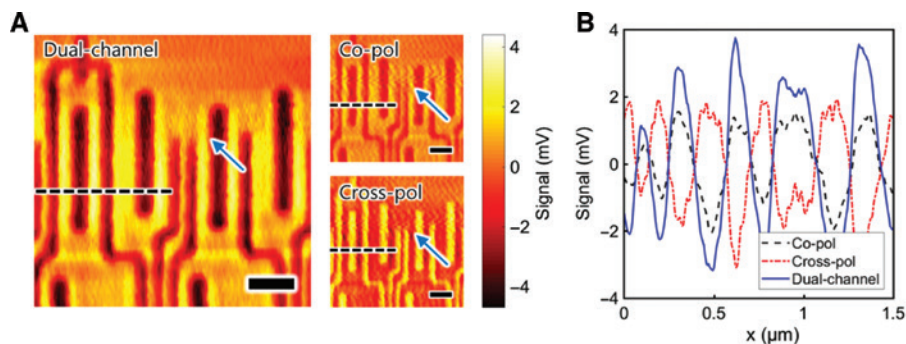


Figure 5: Imaging results of the SiO_2/air heterogeneous structure in dynamic random access memory (DRAM) patterns using the plasmonic near-field scanning nanoscope (PNSN).

(A) Two-dimensional signal maps of a $3\ \mu\text{m} \times 3\ \mu\text{m}$ area through dual-channel detection (left); copolarization signal (right, top); and cross-polarization signal (right, bottom). Crease-like noise artifacts in single-channel images, indicated by blue arrows, are nearly eliminated in the dual-channel case. Scale bar = $0.5\ \mu\text{m}$. (B) Line profiles of black dashed lines.

dual-channel signal shows a clearer outline of the patterns and a higher contrast between the peak and valley of the sample. At the same time, we can identify that the motional artifacts marked by the blue arrow are missing in the dual-channel image and appear as a scratched line in the copolarization and cross-polarization images. This shows that the processing of the dual-channel signal successfully cancels out the motional noise of the probe. We analyzed this marked area quantitatively and obtained 25% reduced motional noise and a two times larger peak-to-valley value, thus gaining a 2.7 times enhanced SNR value on average.

The motional noise was calculated with respect to the root mean square error values of the signal in the y -direction. Furthermore, we showed this SNR enhancement more clearly by comparing the line profiles of the black dashed lines in Figure 5B. The signal differences which indicate the contrast of the dual-channel signal (blue

solid line) are much larger than the copolarization signal (black dashed line). Especially, the signal differences of the cross-polarization signal (red dash-dot line) show an opposite trend to those of the copolarization signal; this directly demonstrates our expectation about the characteristics of the anisotropic reflection signals for the same change in the resonance conditions.

We continuously demonstrated the performance of SNR enhancement in much noisier conditions to confirm the robustness of the dual-channel detection by measuring the dense line array pattern using external vibrations, as shown in Figure 6. Although it is difficult to discern a line pattern in a two-dimensional signal map of an individual single polarization signal, especially a copolarization signal, we can identify a clearer line pattern in a dual-polarization image, as shown in Figure 6A. This is more evident in the line profile of Figure 6B. The line profile of the copolarization signal (black dashed line)

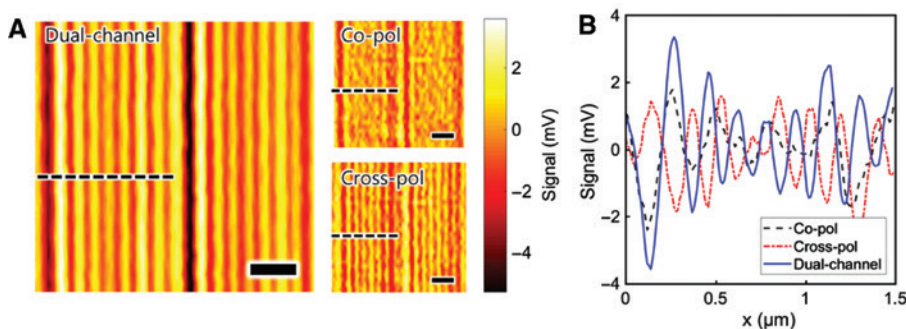


Figure 6: Imaging results of the SiO_2/air line array pattern in dynamic random access memory (DRAM) patterns using the plasmonic near-field scanning nanoscope (PNSN) in noisy conditions.

(A) Two-dimensional signal maps of a $3\ \mu\text{m} \times 3\ \mu\text{m}$ area through dual-channel detection (left); copolarization (right, top); and cross-polarization signals (right, bottom). Scale bar = $0.5\ \mu\text{m}$. (B) Line profiles of black dashed lines.

nearly lost the pitches of the line array, especially in the high spatial resolution; however, the cross-polarization signal (red dash-dot line) shows much clearer line pitches. In addition, the subtracting process successfully cancelled out the noisy signals of each polarization signal. For the entire area, the SNR values of the dual-channel signal were 4.9 times larger than the copolarization signal, due to the 44% reduced noise and 2.7 times larger signal on average.

4 Conclusions

We demonstrated a PNSN using the cross-polarization technique. Assuming that cross-polarization reflection is a radiation from an oscillating resonance current around the aperture, we introduced an equivalent circuit model to analyze the characteristics of the interaction between the aperture and light. Based on the transmission line theory, we defined the anisotropic reflection signal for the copolarization and cross-polarization. In addition, to predict the anisotropic reflection signal quantitatively and confirm the opposite trend, which is key to enhancing the SNR of the detection system, we analyzed each polarization component of the signal with respect to the change in the refractive index of the output space. By defining a PNSN signal for each polarization, we also reduced the motional noise of the probe. The overall performance of the SNR enhancement is demonstrated by the comparison of the two-dimensional images of the dual-channel signal and both the single polarization signals with discussions about the opposite behavior between each polarization component of the anisotropic reflection signal. To verify the individual improvement of contrast enhancement and noise reduction, we analyzed the signals quantitatively. Finally, by using the dual-channel detection system of PNSN, which detects the anisotropic reflection signal, we obtained a 2.7-times higher SNR compared with the copolarization signal in normal operation conditions, and a 4.9 times higher SNR in additional vibration conditions.

5 Supplementary material

The supplementary material is available online on the journal's website or from the author.

Conflicts of interest: The authors declare no conflicts of interest.

References

- [1] Guo H, Meyrath TP, Zentgraf T, et al. Optical resonances of bowtie slot antennas and their geometry and material dependence. *Opt Express* 2008;16:7756–66.
- [2] Kinzel EC, Xu X. Extraordinary infrared transmission through a periodic bowtie aperture array. *Opt Lett* 2010;35:992–4.
- [3] Harris JS, O'Sullivan T, Sarmiento T, Lee MM, Vo S. Emerging applications for vertical cavity surface emitting lasers. *Semicond Sci Tech* 2011;26:014010.
- [4] Ding L, Qin J, Guo S, Liu T, Kinzel E, Wang L. Resonant effects in nanoscale bowtie apertures. *Sci Rep* 2016;6:277254.
- [5] Kim Y, Kim S, Jung H, Lee E, Hahn JW. Plasmonic nano lithography with a high scan speed contact probe. *Opt Express* 2009;17:19476–85.
- [6] Cheng Y-T, Takashima Y, Yuen Y, Hansen PC, Leen JB. Ultra-high resolution resonant C-shaped aperture nano-tip. *Opt Express* 2011;19:5077–85.
- [7] Kim S, Jung H, Kim Y, Jang J, Hahn JW. Resolution limit in plasmonic lithography for practical applications beyond $2 \times$ nm half pitch. *Adv Opt Mater* 2012;24:337–44.
- [8] Lu G, Li W, Zhang T, et al. Plasmonic-enhanced molecular fluorescence within isolated bowtie nano-apertures. *ACS Nano* 2012;6:1438–48.
- [9] Berthelot J, Aćimović SS, Juan ML, Kreuzer MP, Renger J, Quidant R. Three-dimensional manipulation with scanning near-field optical nanotweezers. *Nat Nanotechnol* 2014;9:295–9.
- [10] Verschuere DV, Pud S, Shi X, de Angelis L, Kuipers L, Dekker C. Label-free optical detection of DNA translocations through plasmonic nanopores. *ACS Nano* 2019;13:61–70.
- [11] Lee T, Lee E, Oh S, Hahn JW. Imaging heterogeneous nanostructures with a plasmonic resonant ridge aperture. *Nanotechnology* 2013;24:145502.
- [12] Lee T, Oh S, Hahn JW. Thickness measurements of metal thin films with a plasmonic near-field scanning nanoscope using a resonant ridge aperture. *J Nanophotonics* 2014;8:083075-1–083075-9.
- [13] Morgan SP, Stockford IM. Surface-reflection elimination in polarization imaging of superficial tissue. *Opt Lett* 2003;28:114–6.
- [14] Jacques SL, Roman JR, Lee K. Imaging superficial tissues with polarized light. *Lasers Surg Med* 2000;26:119–29.
- [15] Morgan SP, Zhu Q, Stockford IM, Crowe JA. Rotating orthogonal polarization imaging. *Opt Lett* 2008;33:1503–5.
- [16] Gladkova N, Streltsova O, Zagaynova E, et al. Cross-polarization optical coherence tomography for early bladder-cancer detection: Statistical study. *J Biophotonics* 2011;4:519–32.
- [17] Bozhevolnyi SI, Xiao M, Keller O. External-reflection near-field optical microscope with cross-polarized detection. *Appl Opt* 1994;33:876–80.
- [18] Hong X, van Dijk EMPH, Hall SR, Götte JB, van Hulst NF, Gersen H. Background-free detection of single 5 nm nanoparticles through interferometric cross-polarization microscopy. *Nano Lett* 2011;11:541–7.
- [19] Esslinger M, Dorfmueller J, Khunsin W, Vogelgesang R, Kern K. Background-free imaging of plasmonic structures with cross-polarized apertureless scanning near-field optical microscopy. *Rev Sci Instrum* 2012;83:033704-1–033704-6.

- [20] Miles BT, Robinson EC, van Dijk EMHP, Lindsay ID, van Hulst NF, Gersen H. Sensitivity of interferometric cross-polarization microscopy for nanoparticle detection in the near-infrared. *ACS Photonics* 2015;2:1705–11.
- [21] Wen J, Banzer P, Kriesch A, Ploss D, Schmauss B, Peschel U. Experimental cross-polarization detection of coupling far-field light to highly confined plasmonic gap modes via nanoantennas. *Appl Phys Lett* 2011;98:101109-1–101109-3.
- [22] Kakko J-P, Matikainen A, Anttu N, et al. Measurement of nanowire optical modes using cross-polarization microscopy. *Sci Rep* 2017;7:17790.
- [23] Nahata A, Linke RA, Ishi T, Ohashi K. Enhanced nonlinear optical conversion from a periodically nanostructured metal film. *Opt Lett* 2003;28:423–5.
- [24] Schön P, Bonod N, Devaux E, et al. Enhanced second harmonic generation from individual metallic nanoapertures. *Opt Lett* 2010;35:4063–5.
- [25] Park S, Hahn JW, Lee JY. Doubly resonant metallic nanostructure for high conversion efficiency of second harmonic generation. *Opt Express* 2010;20:4856–70.
- [26] Mivelle M, Ibrahim IA, Baida F, et al. Bowtie nano-aperture as interface between near-fields and a single-mode fiber. *Opt Express* 2010;18:15964–74.
- [27] Yang J, Zhang J. Nano-polarization-converter based on magnetic plasmon resonance excitation in an l-shaped slot antenna. *Opt Express* 2013;21:7934–42.
- [28] Porterfield DW, Hesler JL, Densing R, Mueller ER, Crowe TW, Weikle RM II. Resonant metal-mesh bandpass filters for the far infrared. *Appl Opt* 1994;33:6046–52.
- [29] Cetin AF, Turkmen M, Aksu S, Etezadi D, Altug H. Multi-resonant compact nanoaperture with accessible large nearfields. *Appl Phys B* 2015;118:29–38.

Supplementary Material: The online version of this article offers supplementary material (<https://doi.org/10.1515/nanoph-2019-0132>).